Jouini, H.; Mejri, I.; Martinez-Ortigosa, J.; Cerrillo, JL.; Petitto, C.; Mhamdi, M.; Blasco Lanzuela, T.... (2022). Alkali poisoning of Fe-Cu-ZSM-5 catalyst for the selective catalytic reduction of NO with NH3. Research on Chemical Intermediates. 48(8):3415-3428. https://doi.org/10.1007/s11164-022-04768-9

Alkali poisoning of Fe-Cu-ZSM-5 catalyst for the selective catalytic reduction of NO with NH_3

Houda Jouini [1,2] · Imène Mejri [1,2] · Joaquin Martinez-Ortigosa [3] · Jose L. Cerillo [3] · Carolina Petitto[4] · Mourad Mhamdi [1, 2] · Teresa Blasco [3] · Gérard Delahay [4]

[1] Université de Tunis El Manar, Faculté des Sciences de Tunis, LR01ES08 Laboratoire de Chimie des Matériaux et Catalyse, 2092, Tunis, Tunisie.

[2] Université de Tunis El Manar, Institut supérieur des technologies médicales de Tunis, 1006, Tunis, Tunisie.

[3] Instituto de Tecnología Química, Universitat Politècnica de València - Consejo Superior de Investigaciones Científicas (UPV-CSIC), Avda. de los Naranjos s/n, 46022 Valencia, Spain.

[4] ICGM, Université de Montpellier, CNRS, ENSCM, Montpellier, France.

Houda Jouini

+216 99 92 56 55

houda.jouini@fst.utm.tn

Abstract

Fe (2wt%)-Cu (1.5wt%)-ZSM-5 SCR catalyst was contacted 1.5 wt% of Na and 1.8 wt% of K in order to simulate poisoning by species more specifically contained in exhaust gases from exhaust gases of Diesel engines and power plants. Poisoning agents do not cause loss of surface area nor pore occlusion. XRD and SEM results showed that alkali metals introduction did not deteriorate the crystallinity and morphology of zeolite crystals. However, a significant loss of surface acidity was observed upon alkali-poisoned catalysts causing a dramatic deactivation of the NH_3-SCR of NO reaction. Na-doped catalyst showed higher low-

temperature SCR activity while potassium has a stronger deactivation effect on Fe-Cu-ZSM-5 than sodium beyond 400 °C.

Keywords Alkali metals; Deactivation; NH_3-SCR; NO; ZSM-5.

Introduction

Metal exchanged zeolite SCR catalysts, are among the most effective systems for nitrogen oxides (NOx) abatement from exhaust gases of Diesel engines and power plants providing reduction of NOx emissions up to 99% [1-3]. The durability of this category of catalysts dedicated to automotive applications regarding hydrothermal aging and chemical deactivation must be proven over the lifetime of the vehicle. These requirements are much more stringent than for stationary applications, since the catalysts are exposed to severe conditions: vibrations, high and varying exhaust temperatures, and deactivation by water and by different substances in the exhaust gas, which deposit on the catalyst surface [4-7]. Fuel and lubrication oil additives may contain significant amounts of alkali metals [8]. Their deposition can significantly reduce the performances of the SCR catalysts since they may plug the pores of the catalyst channels and neutralize the Brönsted acid sites, thus decreasing the adsorption sites for ammonia, which play a crucial role in the NH_3-SCR mechanism [9].

Although several studies have been devoted to study the effect alkali metals on commercial vanadia-based catalysts [10-14], the poisoning effect of alkali metals (Na and K) especially on zeolite based catalysts and mainly for the Fe-Cu-MFI system have seldom been reported. In this work, the effect of addition of potassium or sodium and on the SCR activity of Fe-Cu-ZSM-5 catalyst was investigated. Modifications of physico-chemical and catalytic properties occurring upon poisoning have been investigated in order to define a correlation between the alterationof catalysts textures, metal speciation and acidity by alkali metals and their SCR activity.

Experimental

Catalyst preparation

Fe (2wt%)-Cu (1.5wt%)-ZSM-5 sample was prepared by consecutive solid-state ion exchange starting from commercial NH_4^+-ZSM-5 (Si/Al=15) furnished by Zeolyst International (CBV3024E) as follow: 1 g of zeolite was mixed and finely ground with the desired amount of $CuCl_2$*$2H_2O$ (Sigma-Aldrich) in an agate mortar for 5 min under ambient conditions. The resulting mixture was then treated under a stream of helium (99.99%, Air Liquide, 30 cm^3 min^{-1}) for 12 h at 380 °C (2 °C min^{-1}). The obtained powder was mixed and finely ground with the desired amount of $FeCl_2$*$6H_2O$ (Sigma-Aldrich), then heated for 12 h at 290 °C in a stream of helium and under the same conditions described previously.

Catalyst poisoning

The alkali-poisoned samples were prepared by impregnating the aqueous solutions of NaCl (1.5 wt% Na) and KCl (1.8 wt% K) furnished by Sigma-Aldrich onto the fresh Fe-Cu-ZSM-5 catalyst powder for 4h under continuous stirring at ambient temperature. The obtained mixture was then dried overnight at 110°C. The prepared catalysts were denoted: Fe-Cu-Z, Na-Fe-Cu-Z and K-Fe-Cu-Z.

Activity measurements

The NH_3-SCR of NO catalytic test was performed in temperature programmed surface reaction (TPSR) using a flow reactor operating at atmospheric pressure with a space velocity of 333,333 h^{-1} and a total flow rate of 6 L h^{-1}. The concentrations of NH_3 and NO were established from initial gas cylinders containing 0.75% of NH_3/He and 0.75% of NO/He. 18 mg of each sample were activated in-situ at 250 °C under oxygen and helium mixture (8% O_2/He) and then cooled to 200 °C. After reaching the starting reaction temperature, a by-pass of the reactor is done. From this step, the gas outlet composition was continuously monitored

by vacuum stripping a fraction of the exit gas with a capillary towards the mass spectrometer (Pfeiffer Omnistar) equipped with Channeltron and Faraday detectors (0-200 amu) following the characteristic masses of: NH_3 (m/z =15, NH^+), H_2O (m/z =18, H_2O^+), N_2 (m/z = 28, N_2^+), NO (m/z = 30, NO^+) and N_2O (m/z = 44, N_2O^+). Firstly, baselines of NH_3, N_2, NO and N_2O have been set under the mixture containing He, O_2 and water only (3.5% H_2O, 8% O_2 and 88.5% He). Then, the adequate flowrates of 0.75% NO/He and 0.75% NH_3/He were introduced and the He flowrate were adjusted in order to obtain the following gas composition: 1000 ppm of NO and 1000 ppm of NH_3. After attaining the stability of all characteristic mass lines, NO and NH_3 were introduced (mass flowmeters) and by adjusting the He flow, the reaction mixture is ready. Then, the by-pass is removed and the reaction mixture starts to pass through the catalyst. After 10 minutes of dwell, the temperature was increased from 200 °C to 550 °C. The catalytic results were expressed as follows:

Conversion of the reactant R (R=NO or NH_3):

$X_R = \frac{[R_0]-[R_T]}{[R_0]} \times 100$, where $[R_0]$ and $[R_T]$ are the concentrations of the reactant R at the inlet gas reactor and at the temperature T, respectively.

Amount of N_2O formed:

$Q_{N_2O} = \frac{[N_2O_T]-[N_2O_{inj}]}{[N_2O_0]-[N_2O_{inj}]} \times 1000$, where $[N_2O_{inj}]$ is the concentration of N_2O before injection, $[N_2O_T]$ and $[N_2O_0]$ represent the concentrations of N_2O at the temperature T and at the inlet gas reactor, respectively.

Selectivity toward N_2:

$$S_{N_2} = \frac{\left[(X_{NO} \times 1000) + (X_{NH_3} \times 1000)\right] - Q_{N_2O}}{(X_{NO} \times 1000) + (X_{NH_3} \times 1000)} \times 100$$

Catalyst characterization

The chemical analysis of the studied materials was carried out by ICP-AES in a Varian 715-ES spectrometer. The powder samples (ca 20-30 mg) were dissolved in an acid mixture of 20% HNO_3: 20% HF: 60% HCl (% vol) and aged during 24 h. The calibration curve was fitted to the predicted approximate concentration of analyse and determined using standard solutions (Sigma-Aldrich). The wavelengths used for Cu and Fe analysis were 327.395 and 234.350 nm, respectively. N_2 physisorption measurements were determined with an automatic ASAP 2020 apparatus from Micromeritics. Before the nitrogen adsorption, the samples were outgassed at 250 °C until a static vacuum of 3×10^{-5} bar was reached. BET model was used to calculate the specific surface areas, while pore volumes were calculated at the end of the step corresponding to the filling of the pores (at P/P°=0.98). STEM observations were performed using a JEOL-JEM 2100F instrument equipped with an X-MAX microanalysis detector and operating under an accelerating voltage of 200 kV and a resolution energy of 20 eV. The morphology of samples was observed by FE-SEM on a ZEISS AURIGA 55 Compact instrument in combination with an EDX detector. The sample powder was deposited in double-sided tape and analysed without metal covering. The samples crystallinity was checked using a PANanlytical Cubix'Pro diffractometer equipped with an X'Celerator detector using Cu-Kα radiation (0.154056 nm). The equipment is working under a voltage of 45 kV and a current of 40 mA. The diffractograms were recorded in the region of 5-40° and were exploited with the software PANalytical X'Pert HighScore Plus. The phase identification was accomplished by comparing the experimental diffractograms with the references of the international database ICDD (The International Centre for Diffraction Data). XPS analyses were performed using a SPECS spectrometer equipped with a MCD-9 detector. The source is composed of an aluminium anode emitting a monochromatic X-ray radiation (Kα = 1486.6 eV). NH_3-TPD profiles were obtained on an automated Micromeritics Autochem II analyser.

Before NH_3-TPD measurements, samples (50 mg) were pre-treated in a quartz U-tube reactor under air flow (10 cm^3 min^{-1}) at 500 °C (10 °C min^{-1}) for 1 hour and then cooled under helium (100 cm^3 min^{-1}) to 100 °C. The ammonia was adsorbed (10 cm^3 min^{-1}) during 1 hour then adsorbed under helium atmosphere (100 cm^3 min^{-1}) to 800 °C (10 °C min^{-1}). DRS UV-vis measurements were performed on a Perkin Elmer Lambda 45 spectrophotometer equipped with a diffuse reflectance attachment. Spectra were recorded at room temperature in the wavelength range of 200-900 nm using $BaSO_4$ as reference material.

Results and discussion

Physico-chemical characterisation

The chemical analysis was performed by ICP-AES technique. Obtained results are gathered in Table 1 including Fe, Cu, Na and K contents. Examination of ICP results shows that metals are well retained by the zeolite during the preparation process where the experimental amounts approximate the theoretical values set for the catalysts preparation.

Table 1

ICP-AES chemical analysis and N_2 physisorption at 77 K results.

Sample	Fe (wt%)	Cu (wt%)	Na/K (wt%)	S_{BET} [a] (m^2/g)	Pore volume [b] (cm^3/g)	Micropore volume [c] (cm^3/g)
NH_4^+-ZSM-5	-	-	-	336	0.15	0.12
Fe-Cu-Z	1.83	1.40	-	327	0.13	0.11
Na-Fe-Cu-Z	1.79	1.22	1.42	311	0.17	0.12
K-Fe-Cu-Z	1.79	1.24	1.79	347	0.14	0.10

[a] calculated by BET method, [b] calculated by BJH method, [c] calculated by t-plot method

XRD patterns of unpoisoned catalyst show the typical signals of parent zeolite as shown in Figure 1. No signals attributable to the Fe and/or Cu oxide aggregates suggesting a good

dispersion of the active phases. The principal diffraction peaks intensities of the parent zeolite decreased with metals addition due to the higher absorption coefficient of copper and iron compounds for the X-ray radiation [15].

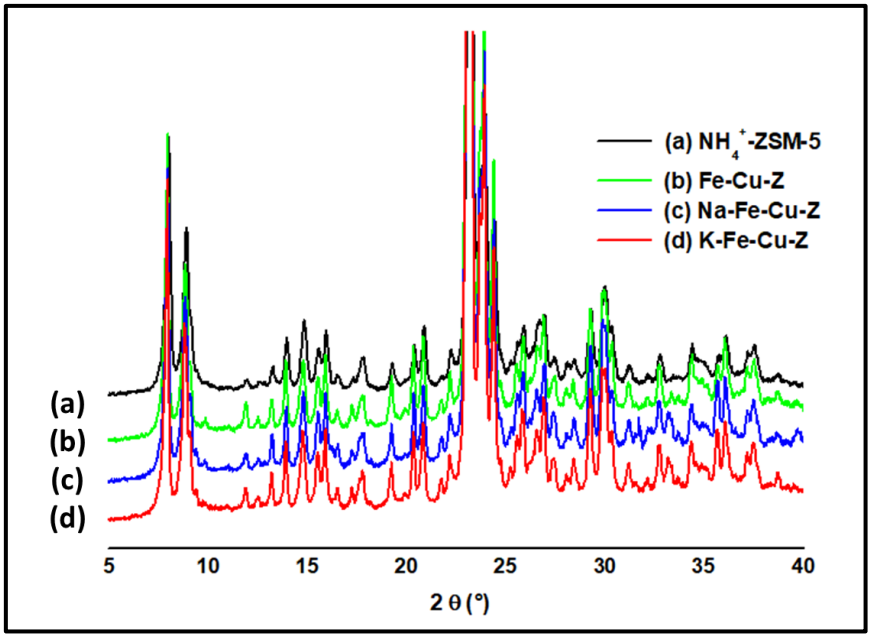

Fig. 1 XRD diffractograms of prepared catalysts.

XRD patterns of poisoned samples are superimposable to those of the corresponding pure catalyst suggesting that no detectable formation of alkaline metal oxides occurs. A negligible effect of poisoning agents on the surface area of the samples was also observed (Table 1). The S_{BET} of K-poisoned sample was slightly improved suggesting a partial modification of the external surface of the catalyst. Pore size distribution confirms that no significant pore blocking occurs upon poisoning.

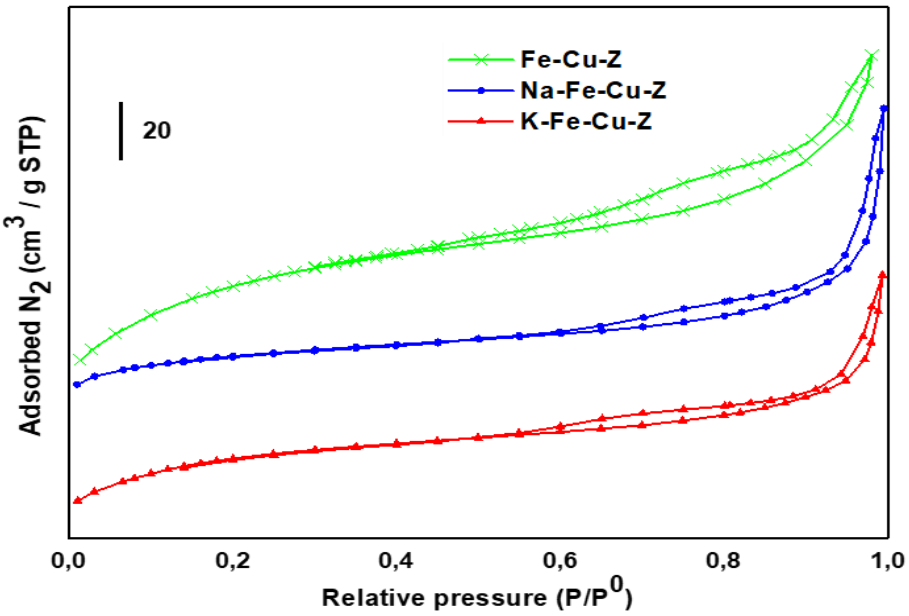

Fig. 2 N_2 Adsorption-desorption isotherms of prepared catalysts.

The porosity of zeolite nanoparticles before and after poisoning treatment was investigated by N_2 sorption analysis (Fig.2). The nitrogen adsorption isotherm of fresh Fe-Cu-Z was basically type I according to the classification of IUPAC. Predominant adsorption ended below P/P^0 = 0.02, which is a characteristic of uniform microporous solids. Both alkaline-treated samples have the same predominant adsorption ended below P/P^0 = 0.02 as the fresh sample, indicating the preservation of microporosity, while their isotherms show an uptake rise and a change in the shapes of hysteresis loops (Type H3) extending from P/P^0 = 0.4 to nearly 1, indicating the creation of mesoporosity formed by the packing of zeolite nanocrystals due to poisoning treatment [16].

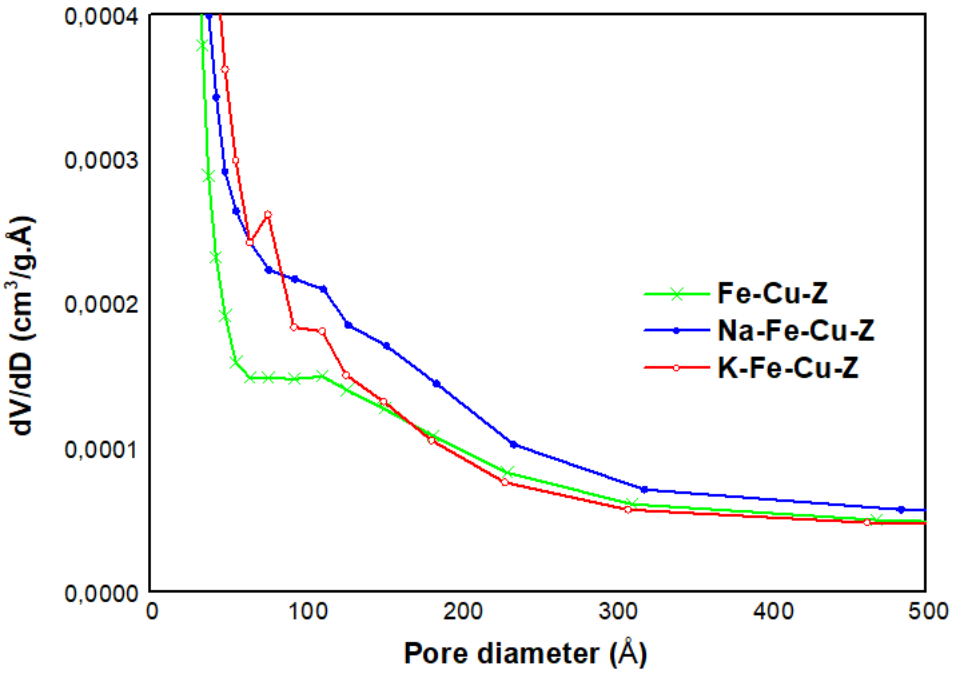

Fig. 3 BJH adsorption pore-size distribution (PSD) of prepared catalysts according to Harkins-Jura method.

Comparison of the PSD of the fresh and alkaline-treated catalysts derived from the adsorption branch (Figure 3) shows that The distribution is relatively broad in the case of poisoned samples as can be expected from the proposed mechanism of mesopore formation according to Ogura et al [17]. A pronounced peak centered around 75 Å (7.5 nm) for only K-Fe-Cu-Z sample indicting the formation of new mesopores upon potassium treatment. Development of extra-porosity is normally achieved by application of alkaline treatments mainly causing Si remove from the zeolite framework [18]

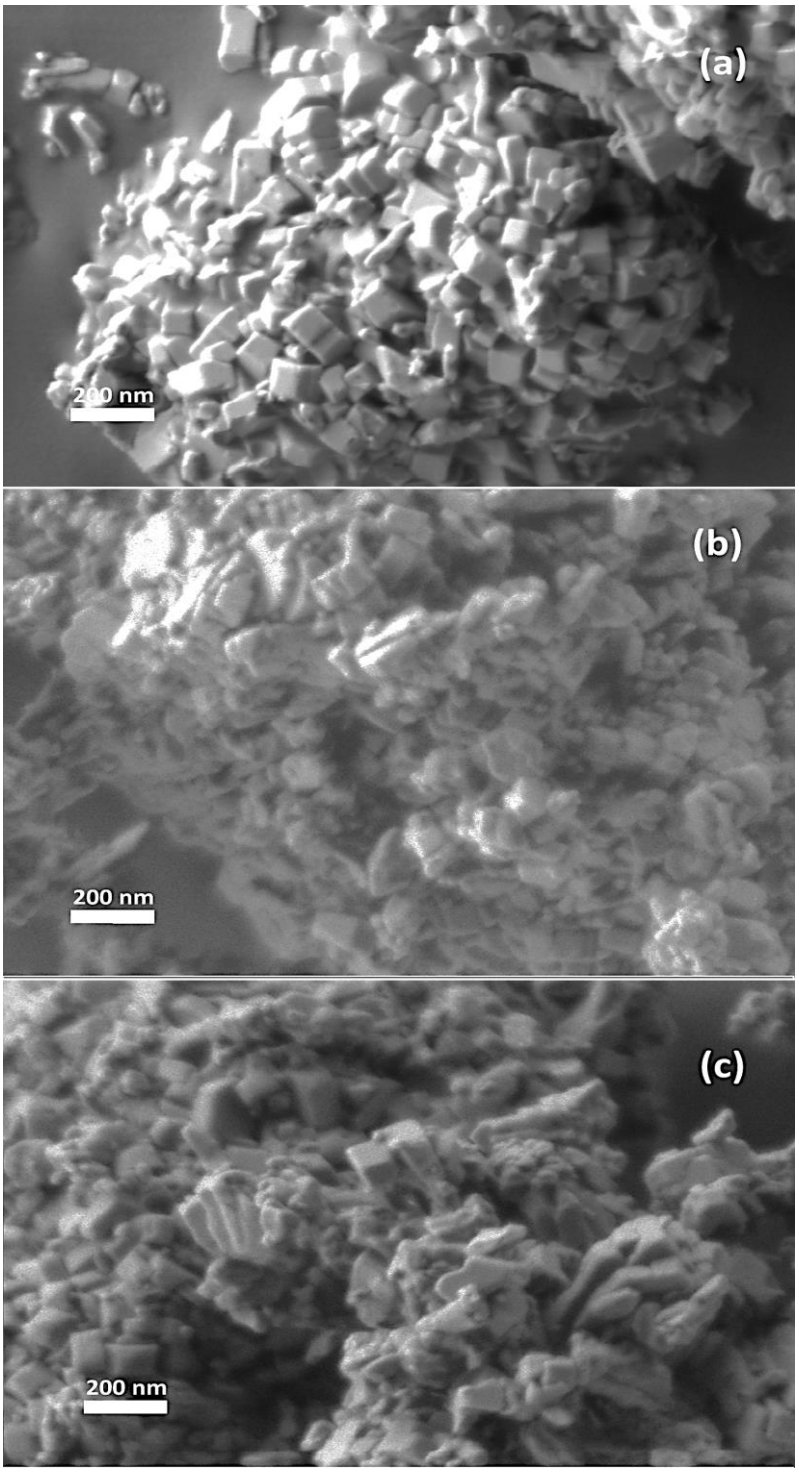

Fig. 4 SEM micrographs in the magnitude 50000x of Fe-Cu-Z (a), K-Fe-Cu-Z (b) and Na-Fe-Cu-Z (c).

SEM/EDX analysis was performed on the studies catalysts and the obtained micrographs were presented in Figure 4 showing that the morphology was not modified by poisoning as concerns both shape and dimension of catalyst particles.

Figure 5 shows STEM micrographs of the catalysts. The distribution of copper and iron species were studied by EDX elemental analysis showing that nano-sized metal species (<100 nm) were formed. The size of the particles indicate that they are located on the outer surface of the zeolite [16]. STEM image of Fe-Cu-Z (Fig. 5a), showed highly dispersed iron particles (spectra 25, 26 and 27) with a size of 8-20 nm. They coexist with smaller Fe-Cu nanocomposites (spectrum 22) as confirmed by EDX analysis with an average size of 3 nm. In the case of Na-Fe-Cu-Z (Fig. 5b), larger iron oxide particles (30-60 nm) are observed (spectra 26 and 29) together with large copper oxide particles (40 nm) and Fe-Cu nanocomposites (spectra 27 and 28) of about 12 nm. EDX analysis showed that metal species are rather agglomerated compared to the fresh sample. The STEM micrograph of K-Fe-Cu-Z (Fig. 5c) showed differently sized iron oxide particles (8-88 nm) with a rather uniform distribution. A limited number of Fe-Cu nanocomposites was detected for this catalysts with an average size of 8 nm (spectrum 22).

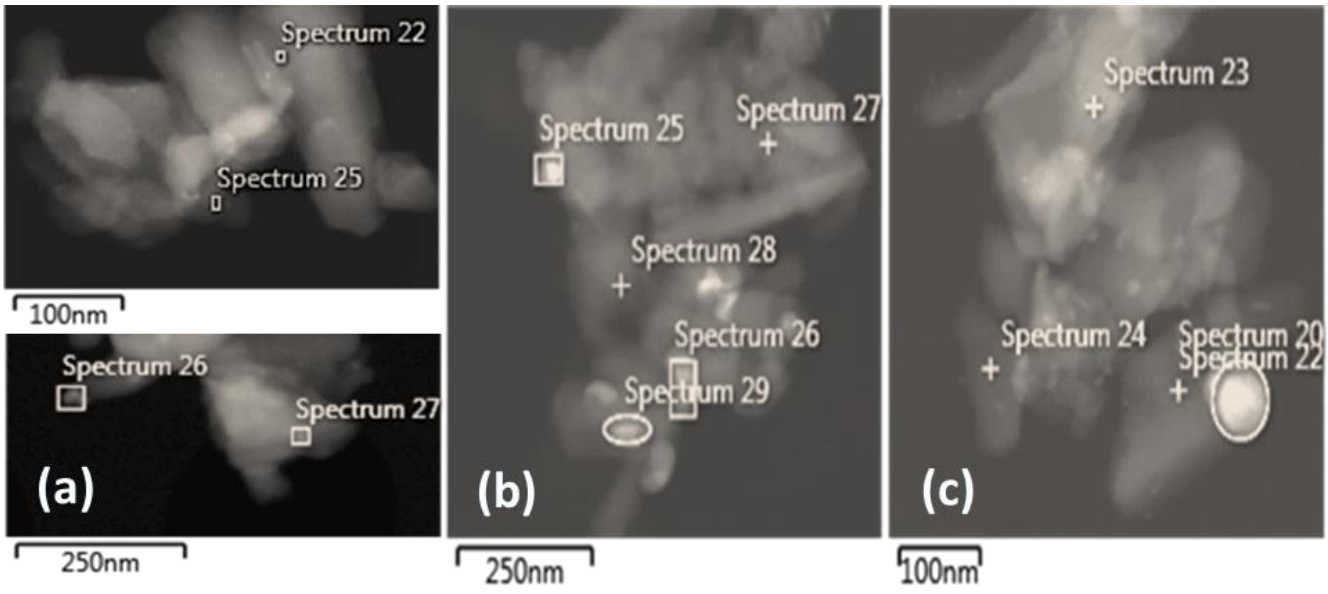

Fig. 5 STEM micrographs of Fe-Cu-Z (a), K-Fe-Cu-Z (b) and Na-Fe-Cu-Z (c).

It can be concluded that sodium deposition promotes the aggregation of copper species while potassium deposition promotes the aggregation of iron particles. In addition, while potassium is uniformly distributed, sodium is more concentrated on the catalysts particles.

Table 2

EDX elemental analysis results

Sample	Spectrum	Element (wt%)						
		O	Al	Si	Cl	Fe	Cu	Na/K
Fe-Cu-Z	22	47.73	1.55	40.31	0.40	1.60	8.41	-
	25	54.85	0	26.32	0.33	18.50	0	-
	26	46.15	0	12.44	0.18	41.22	0	-
	27	51.87	1.95	33.41	1.18	11.59	0	-
Na-Fe-Cu-Z	25	16.15	0	10.22	11.69	0	61.53	0.41
	26	46.72	1.29	21.03	0.26	30.40	0.04	0.26
	27	52.70	2.05	42.89	0.06	0.24	1.29	0.14
	28	47.78	0	49.57	0.07	0.29	2.29	0
	29	46.09	1.19	28.85	0.10	23.21	0.02	0.54
K-Fe-Cu-Z	20	46.71	0.93	17.32	0	34.15	0	0.88
	22	52.01	0	1.43	0.16	0.23	0	0.22
	23	52.12	0	47.32	0	0	0	0.57
	24	39.61	0	39.04	0.2	17.61	0	3.55

The valence and coordination state of Fe and Cu species present in the prepared catalysts were determined by UV-vis spectroscopy. The Kubelka-Munk function was calculated from reflectance measurements and the recorded spectra were shown in Figure 6.

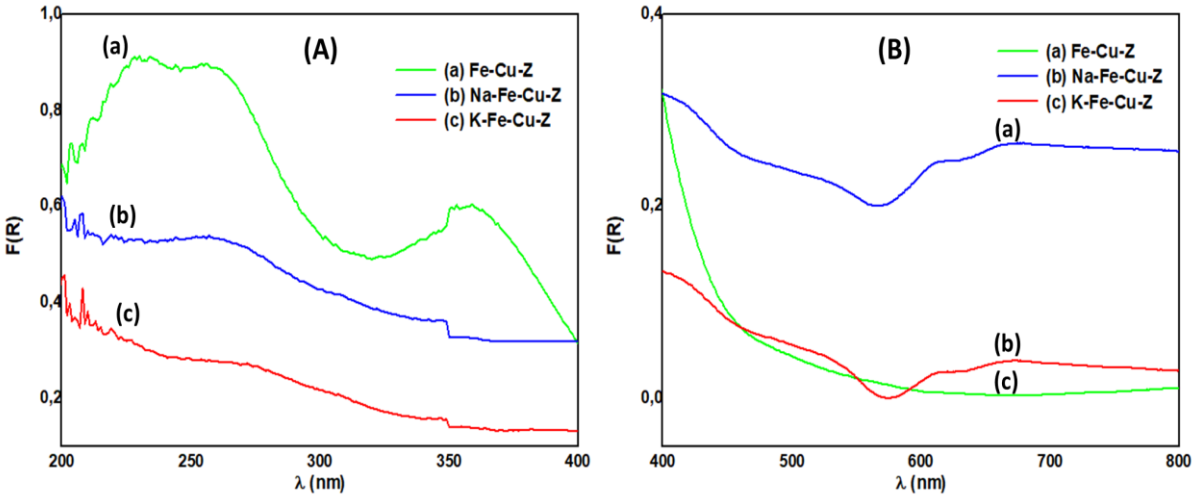

Fig. 6 DRS UV-vis spectra of studied catalysts for wavelength domains: 200-400 nm (A) and 400-800 nm (B).

UV-vis spectrum of the unpoisoned catalysts showed two absorption bands at around 232 and 256 nm: the first is a d-d charge transfer band assigned to Fe^{3+} species in tetrahedral coordination ($e \rightarrow t_2$) [19], while the second originates mainly from the p-d charge transfer transition between framework oxygen and Fe^{3+} cations [20]. Oligonuclear $Fe^{3+}{}_xO_y$ clusters are characterized by bands located in the range of 300-400 nm [21], thus the band appearing at 357 nm was assigned to $Fe^{3+}{}_xO_y$ clusters

Na and K-poisoned samples showed the same UV-vis profile: the p-d charge transfer transition between framework oxygen and Fe^{3+} and the signal of oligonuclear $Fe^{3+}{}_xO_y$ clusters were both detected with a slight bathochromic shift compared to Fe-Cu-Z sample probably due to the difference in the environment of metallic species after the poisoning treatment. Additional broad bands located at $\lambda > 600$ nm (Fig.6(B)) attributable to $t_{2g} \rightarrow e_g$ transitions of Cu^{2+} ions in octahedral symmetry were detected for both poisoned samples only [22].

Temperature programmed desorption of NH_3 (NH_3-TPD) experiments were carried out on the pure catalyst and poisoned samples to determine the amount and strength of their different acid sites. The desorption temperatures determined from the NH_3-TPD analysis and the corresponding amounts of ammonia consumption evaluated from the integration of TPD curves are presented in Table 3.

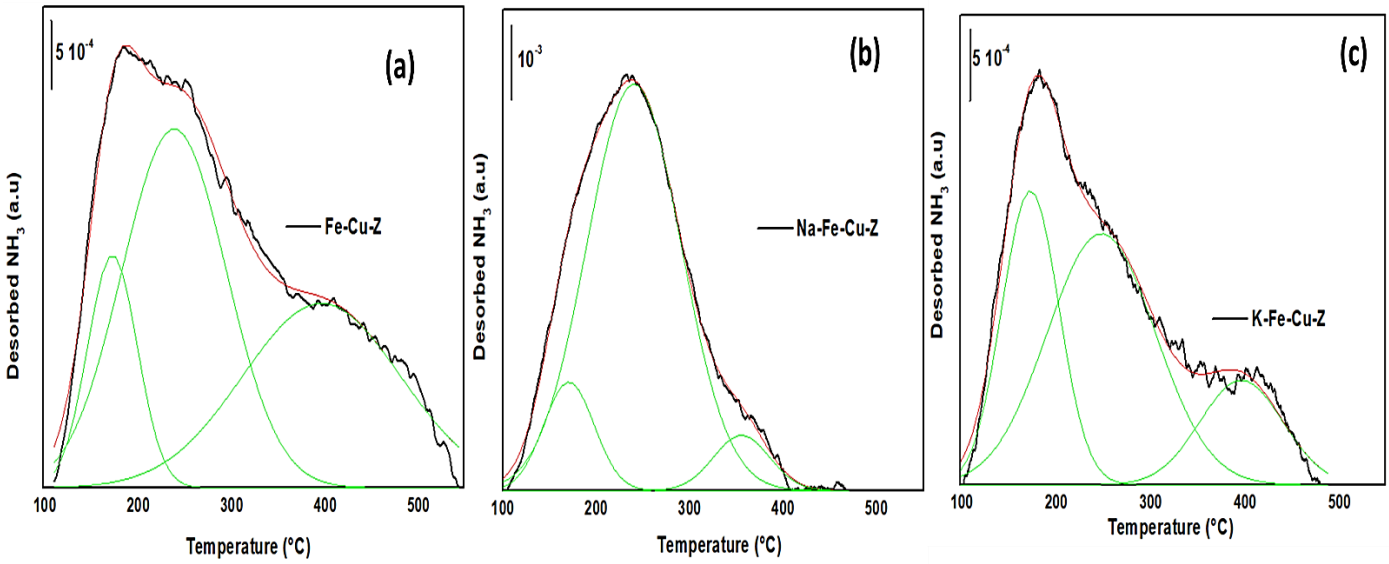

Fig. 7 NH_3-TPD profiles of Fe-Cu-Z (a), K-Fe-Cu-Z (b) and Na-Fe-Cu-Z (c).

Figure 7(a) shows the NH_3-TPD profiles of Fe-Cu-Z. The fresh catalyst exhibits a low temperature peak (peak-l) corresponding to the desorption of weakly chemisorbed ammonia on Lewis and/or weak Brönsted acid sites, or silanol groups [2]. The high temperature peak (peak-h) is assigned to the desorption of strongly chemisorbed ammonia on strong Brönsted acid sites ($Si\text{-}OH^+\text{-}Al$) [2]. The desorption peak located at intermediate temperature (peak-i) is attributed to ammonia desorption from medium-strength acid sites. The deposition of alkali metals substantially reduces surface acidity mainly affecting strong acid sites, which are eliminated of about 85.7 and 74.3 % for Na-Fe-Cu-Z and K-Fe-Cu-Z samplers respectively. The effect of potassium is more pronounced compared to that of sodium on the base of the same molar concentration as it can be noticed from the quantitative study reported in Table 3. K^+ ions easily diffuse into the pore channels of the zeolite [23]. They can thus dislodge and

replace protons and metal ions (Cu or Fe) and therefore induce a consequent decrease in Brönsted acid sites and Lewis sites, respectively [24].

This stronger effect of potassium compared to sodium was also observed by Zhu et al in the NH_3-SCR of NOx over Cu-SSZ-39 [25]. Fan et al., to explain this, proposed that the smaller diameter of hydrated potassium and its higher binding capacity makes its diffusivity much stronger than that of sodium [26]. This finding is in agreement with the higher deactivation effect of potassium observed in ourNH_3-SCR catalytic tests.

The obtained results indicate that the amount of NH_3 adsorption is the major difference between the fresh and poisoned catalysts, which is responsible for the reaction activity. As reported in the literature, alkali metals atoms can directly dislodge the active catalyst sites from exchange sites of the catalyst [27], thus lower the surface acidity by prohibiting ammonia adsorption [12], and change the nature of copper sites.

Table 3

NH_3-TPD quantitative study.

Sample	Acidity [a] (T_{max} [b])				Loss in strong acid sites (%)
	"l" peak	"i" peak	"h" peak	Total	
Fe-Cu-Z	0.14 (174)	0.45 (240)	0.35 (398)	0.94	-
Na-Fe-Cu-Z	0.08 (171)	0.59 (240)	0.05 (355)	0.72	85.71
K-Fe-Cu-Z	0.18 (174)	0.29 (249)	0.09(398)	0.56	74.28

[a] Expressed in mmol of NH_3/g of sample, [b] Temperature of maximum desorption of low (l), intermediate (i) and high (h) peaks expressed in °C

NH_3-SCR catalytic activity

In Figure 8, results of catalytic tests, expressed in conversion of NO as function of temperature, are reported for unpoisoned and alkali poisoned catalysts. The fresh catalyst

achieved above 90 % of NO conversion at 350-500 °C and a weak amount of N_2O was detected for this catalyst compared to the poisoned ones as shown in Figure 8. The NO/NH_3 conversion ratio was close to 1 for the fresh catalyst in the temperature window 425-485 °C and then the conversion of NO slightly decreased of about 5%. A second test on the same aliquot led to the same NO conversion profile (not shown), thus showing the stability of the catalyst and also validating the TPSR method for measuring the NO conversion.

After the addition of alkali metals, both poisoned catalysts were severely deactivated within the whole testing temperature range. The catalyst containing sodium has a better low-temperature SCR activity than that containing potassium. The highest conversion of NO recorded for Na-Cu-Fe-Z was about 93 % around 400 °C. Then this NO conversion first decreases slowly on a window of 50 °C above this temperature and after decreases rapidly to reach 52% at 550 °C, due to strong ammonia oxidation activity. Therefore this NO conversion profile is a volcano-type curve which can be attributed, according to previous studies [28, 29] to copper oxide sintering.

The catalytic profile of the K-doped catalyst exhibits, with respect to Fe-Cu-Z, a loss of conversion into NO of 30-35 % at low temperature, loss which diminishes with the increase of temperature. A maximum of conversion slightly inferior at 90 %. is reached at 470 °C. Above this latter temperature, a weak NO conversion decrease is observed. This conversion decrease follows the same trend as that of the fresh catalyst. Therefore K-Fe-Cu-Z behaves differently than Na-Fe-Cu-Z. The higher loss of activity, at low temperatures, of K-Fe-Cu-Z can be attributed to the stronger aggregation of iron species, observed before for this catalyst (STEM and EDX analyses). On the other hand, the quite stability of the NO reduction activity at temperature above 470°C could be attributed to the better maintain of the copper species at the exchange sites.

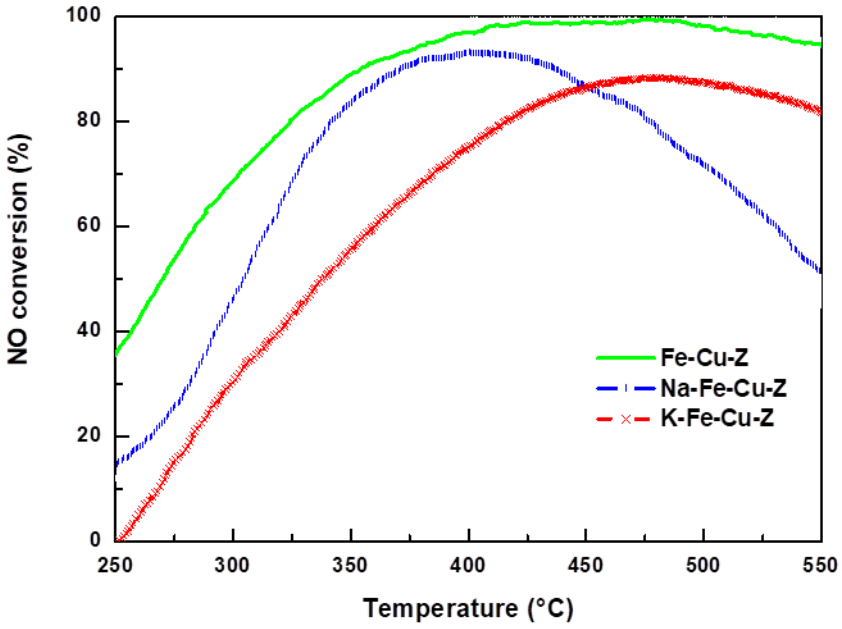

Fig.8 NO conversion over the prepared catalysts.

A good correlation is observed between the SCR activity and the evolution of N_2O^+ fragment intensity (Fig. 9). The Na-poisoned catalysts showed severely worsened high-temperature activity for NO conversion compared to K-Cu-Fe-Z, which was due to an important NH_3 oxidation ($4\ NH_3 + 5\ O_2 \rightarrow 4\ NO + 6\ H_2O$). As regards to the side reactions, the catalysts have tendency to form nitrous oxide ($4\ NH_3 + 4\ NO + 3\ O_2 \rightarrow 4\ N_2O + 6\ H_2O$) at high temperature (> 400 °C) instead of decomposing NO in the presence of NH_3 as a reducing agent [30]

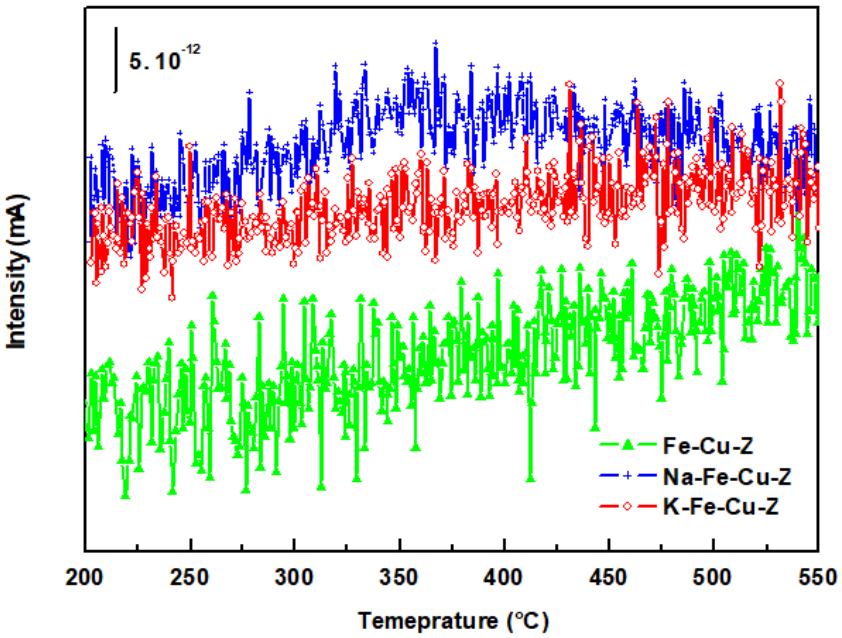

Fig. 9 Evolution of N_2O^+ fragment (m/e=44) intensity over the prepared catalysts.

Discussion

Deposition of small amount of alkaline metals (1.5 wt% of Na and 1.8%wt of K) leads to a dramatic deterioration of catalytic activity and a significant loss of surface acidity compared to fresh Fe-Cu-Z sample. At the same molar concentration of alkali metals, potassium gives rise to a more significant deactivation effect with regard to sodium at the low temperature range, related to its better neutralising properties of acid sites. Strong acid centres adsorbing NH_3 at temperature above 350 °C, which are not involved in the SCR mechanism occurring at lower temperatures, are more neutralised by sodium while the neutralizing effect of potassium affects more medium and weak acid sites leading to a lower catalytic activity compared to the catalyst doped with sodium [11]. The STEM-EDX study revealed the highest aggregation degree of Na-Fe-Cu-Z. Observations on different regions of the sample showed the presence of large iron and copper oxides which may explain the deterioration of the catalyst at high reaction temperature. In fact, the side reaction of ammonia oxidation reaction is promoted by the presence of large metal oxide particles, mainly CuO which was detected only for the Na

doped catalyst [31]. This explains the higher loss of NO conversion observed for Na-Fe-Cu-Z at temperature above 450 °C.

Neither significant structural and textural changes were detected for our catalysts, indicating that deactivation was caused only by changes in the distribution and coordination of iron and/or copper species and mainly on the acidic properties of the catalysts [29,32].

Conclusion

Fe-Cu-ZSM-5 catalysts have been shown excellent SCR activity at the entire temperature range. However, the exhaust gases of Diesel vehicles and some plants contain alkali metal compounds after dust removal, which can have a severe poisoning effect on the activity of Fe-Cu-ZSM-5 catalyst. XRD, SEM and N_2 physisorption characterization results showed that alkali metals introduction did not decrease the crystallinity and textural properties (specific surface area and pore volume) of parent zeolite but induced new mesoporosity to the ZSM-5 material. STEM-EDX and NH_3-TPD showed that Na promotes the agglomeration of iron and copper particles and neutralizes strong acid sites leading to a remarkable deterioration of Na-Fe-Cu-Z catalyst at high temperature range since it is well recognized that the decrease of surface acidity is regarded as one of the main reasons for the deactivation of alkali poisoned catalysts. This study clearly shows that the K-resistance of Fe-Cu-Z was better than Na-resistance above 400 °C which can be attributed to the better strong acidity and dispersion of metallic species of the resulting material after K deposit. Therefore, iron and especially copper are much less back exchanged in the presence of potassium than sodium.

References

1. Jouini H, Martinez-Ortigosa J, Mejri I, Mhamdi M, Blasco T, Delahay G (2019) Res Chem Intermed 45: 1057-1072.

2. Jouini H, Mejri I, Martinez-Ortigosa J, Vidal-Moya A, Mhamdi M, Blasco T, Delahay G (2018) Micropor Mesopor Mater 260: 217-226.

3. Jouini H, Mejri I, Martinez-Ortigosa J, Cerrillo JL, A, Mhamdi M, Palomares AE, Delahay G, Blasco T (2018) Solid State Sci 84: 75-85.

4. Chen G, Xiong S, Chen X, Chu X, Yin R, Liu C, Chen J, Li J (2021) Environ Sci Technol 55: 11368-11374.

5. Ming S, Pang L, Chen Z, Guo Y, Guo L, Liu Q, Liu P, Dong Y, Zhang S, Li T (2020) Micropor Mesopor Mater 303: 110294.

6. Xiong S, Chen J, Huang N, Yan T, Peng Y, Li J (2020) Appl Catal B: Environ 267: 118668.

7. Zhao Y, Shi L, Shen Y, Zhou J, Jia Z, Yan T, Wang P, Zhang T (2022) Environ Sci Technol 56: 4386-4395.

8. Khodayari R, Odenbrand CUI (2001) Appl Catal B: Environ 30: 87-99.

9. Wu Q, Chen X, Mi J, Cai S, Ma L, Zhao W, Chen J, Li J (2021) ACS Sustainable Chem Eng 9: 967-979.

10. Kroöcher O, Elsener M (2008) Appl Catal B: Environ 75: 215-227.

11. Lisi L, Lasorella G, Malloggi S, Russo G (2004) Appl Catal B: Environ 50: 251–258.

12. Peng Y, Li J, Shi W, Xu J, Hao J (2012) Environ Sci Technol 46 : 12623−12629.

13. Feng C, Wang P, Liu X, Wang F, Yan T, Zhang J, Zhou G, Zhang D (2021) Environ Sci Technol 55: 11255-11264.

14. Zhou G, Maitarad P, Wang P, Han L, Yan T, Li H, Zhang J, Shi L, Zhang D (2020) Environ Sci Technol 54: 13314-13321.

15. Qi GS, Yang RT (2005) Appl Catal A: Gen 287: 25-33.

16. Beznis NV, Weckhuysen BM, Bitter JH (2010) Catal Lett 138: 14-22.

17. Ogura M, Kikuchi E, Matsukata M (2001) Stud Surf Sci Catal 135: 216.

18. Suzuki T, Okuhara T (2001) Micropor Mesopor.Mater 43 : 83-89.

19. Pérez-Ramírez J, Groen JC, Brückner A, Kumar MS, Bentrup U, Debbagh MN, Villaescusa LA (2005) J Catal 232: 318-334.

20. Sun K, Fan F, Xia H, Feng Z, Li WX, Li C (2008) J Phys Chem C 112: 16036-16041.

21. Bordiga S, Buzzoni R, Geobaldo F, Lamberti C, Giamello E, Zecchina A, Leofanti G, Petrini G, Tozzola G, Vlaic G (1996) J Catal 158: 486-501.

22. Chanquía CM, Sapag K, Rodríguez-Castellón E, Herrero ER, Eimer GA (2010) Phys Chem Chem Phys 114: 1481-1490.

23. Liu L, Wu X, Ma Y, Ran R, Si Z, Weng D (2020) Catal Surv Asia 24: 250-258.

24. Lisi L, Cimino S (2020) Catalysts 10: 1475-1499.

25. Zhu N, Shan Y, Shan W, Sun Y, Liu K, Zhang Y, He H (2020) Environ Sci Technol 54: 15499–15506.

26. Fan C, Chen Z, Pang L, Ming S, Dong C, Albert KB, Liu P, Wang J, Zhu D, Chen H, Li T (2018) Chem Eng J 334: 344-354.

27. Zhang P, Wang P, Chen A, Han L, Yan T, Zhang J, Zhang T (2021) Environ Sci Technol 55: 11970-11978.

28. Mehsein K, Delahay G,Villain N, Moral N (2019) Int J Automot Mech Eng 16 (3) :6918-6930.

29. Tarot M-L, Iojoiu E E, Lauga V, Duprez D, Courtois X, Can F (2019) Appl Catal B: Environ 250: 355–368.

30. Madia G, Koebel M, Elsener M, Wokaun A (2002) Ind Eng Chem Res 41: 4008-4015.

31. Sjövall H, Olsson L, Fridell E, Blint RJ (2006) Appl Catal B: Environ 64: 180-188.

32. Wu Q, Fan C, Wang Y, Chen X, Wang G, Qin Z, Mintova S, Li J, Chen J (2022) Chem Eng J 435: 134890.